PNAS
www.pnas.org

# Supplementary Information for

## First-principles-based reaction kinetics from reactive molecular dynamics simulations: application to hydrogen peroxide decomposition

Daniil V. Ilyin, William A. Goddard III,* Julius J. Oppenheim, and Tao Cheng

* Email: wag@wag.caltech.edu

**This PDF file includes:**

Supplementary text

Figs. S1 to S9

Captions for movies S1 to S8

Table S1

**Other supplementary materials for this manuscript include the following:**

Movies S1 to S8

**Table of Contents**





www.pnas.org/cgi/doi/10.1073/pnas.1701383115

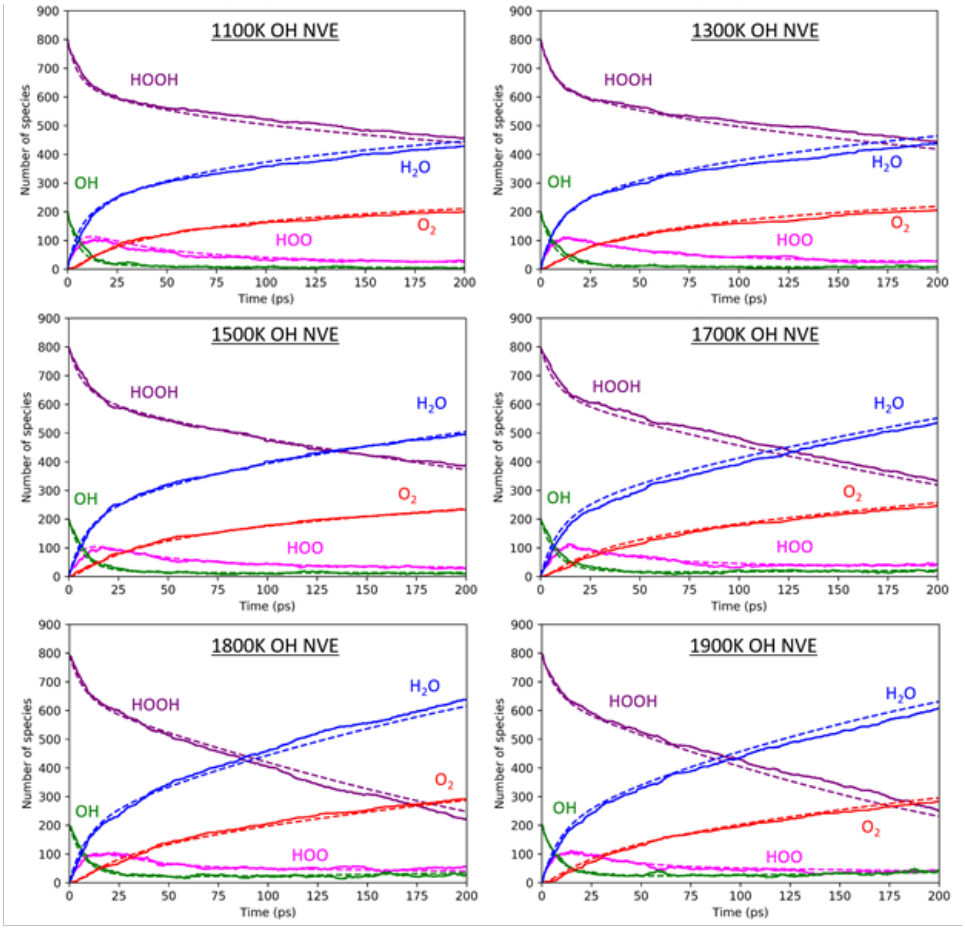


**Figure S1.** Reaction kinetics for OH initiated HOOH decomposition for additional temperatures, at T=1100, 1300, 1500, 1700, 1800, and 1900K

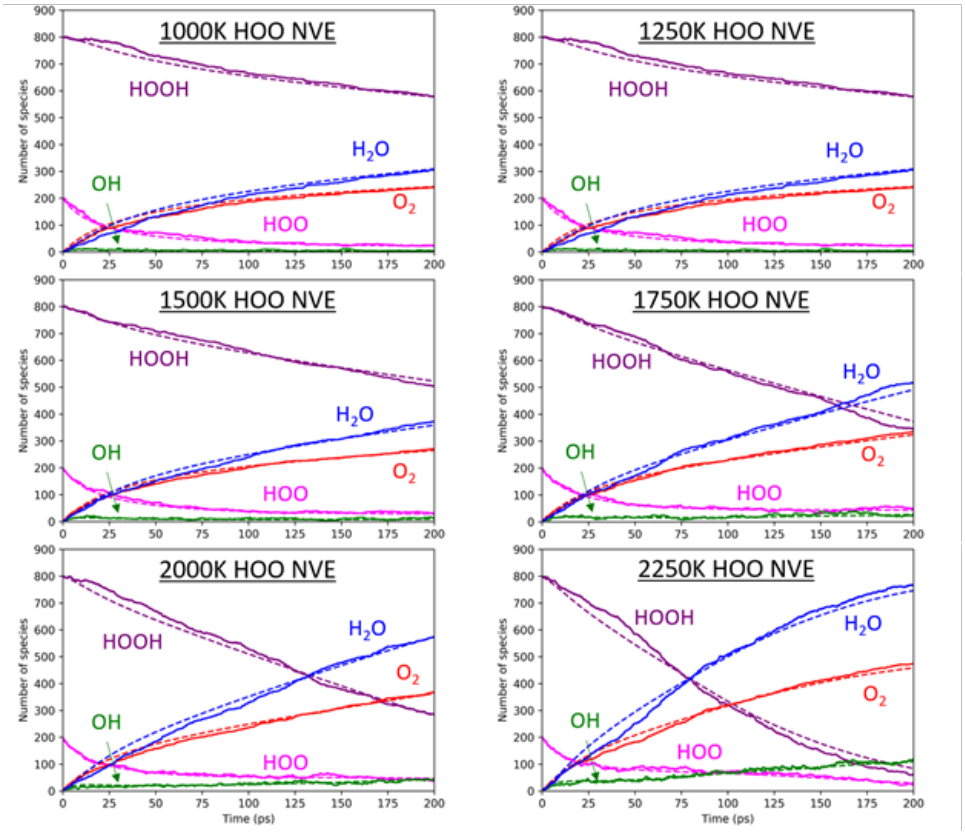


**Figure S2.** Reaction kinetics for HOO initiated HOOH decomposition from 1000K to 2000K in increments of 250K.

This simulation was seeded with HOO radicals and reached a steady state between OH and HOO concentrations after approximately 75 picoseconds. The predicted and observed dynamics are presented in Figure S2. This can be compared with Figure 1 and S1, which seeded the system with OH radicals. The predicted and observed dynamics for both cases are self-consistent. The main difference is in the initial rate of disappearance of HOOH up until the OH-HOO equilibrium point, which is faster in the OH case than in the HOO case. This is explained by the higher reactivity of OH compared to HOO.

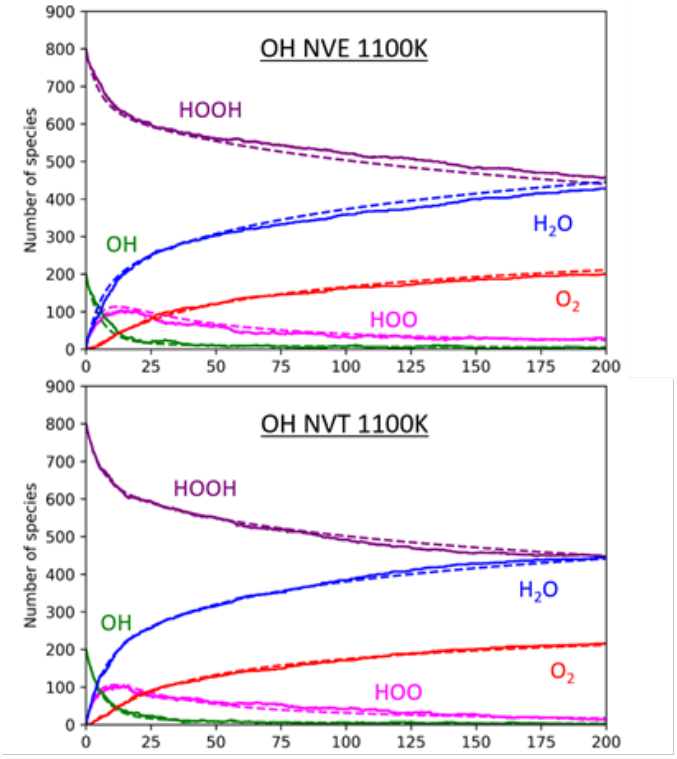


**Figure S3.** Reaction kinetics for OOH and OH initiated HOOH decomposition using NVT and NVE dynamics.

Figure S3 compares the kinetics for OH evolution with NVT fixed at 1100K with NVE starting at 1100K as in S1. In both cases, the extracted kinetics reproduce observed dynamics well.

**Combustion induced interface instability.** Several papers in this issue report on interface instabilities that results from differences in density. For an instability to appear in a chemical reaction, conditions must allow an interface perturbation to grow exponentially. Conversely, if the perturbations dissipate, the evolution of the interface will be stable. In our simulations, we consistently see the formation and dissipation of perturbations.

We show here two systems discussed in the paper: Case 2 and Case 9. Case 2 is a periodic box with dimensions 10nm along x (vertical), 25nm along z (horizontal), and 4 nm along y (out of the page). The system was seeded with a 10x4x4 nm region of pure OH at a density 5 times the bulk density, which is 50 $kg/m^3$.

Figure S4a shows evolution of this system, which is similar to many others that we studied. A few OH radicals consistently shoot out from the seed region into the bulk, where they react and form a region of reactants, intermediates, and products that extend past the initial flat interface: a small perturbation. However, two factors are at play that diminish further propagation. Firstly, the growth of the perturbation along z is hindered beyond the first few collisions due to the small mass of the radicals with little bulk momentum along z. The reactions that occur during the first collisions eject radicals isotropically, so that the energy of the initial perturbation is dissipated rather quickly. Secondly, the conditions of this system are such that each reaction converts one radical to another, lacking the multiplication that might lead to exponential growth of the perturbation.

These results serve to illustrate the dissipative mechanisms that stabilize the Landau-Darrieus instability [41]. There may be other conditions that would result in an exponentially growing instability. For instance, a different initial interface (triangular or sawtooth geometry) may help provide the bulk momentum necessary for perturbation propagation. A different chemistry (more highly reactive species or a much higher temperature) may help with multiplying the number of radicals generated by each reaction, which would help the perturbation grow exponentially. Continuum dynamics simulations could be carried out using the kinetics information extracted from our atomistic simulations to examine larger for longer times that might find the optimum conditions for instabilities.

The geometry of Case 9 is shown in Figure S4b. It is a periodic box 20x2x100 nm with a density of 1400 $kg/m^3$. It is seeded with 5% HOO in a 20x2x2 region on the left. The region of detail for Figure S4c is outlined in red.

The evolution of a perturbation at the interface is shown in Figure S4c. The perturbation occurs due to motion of a few radicals. However, its evolution is hindered. The small initial momentum in z is dispersed due to collisions with the bulk HOOH (present everywhere in the white space, not shown for clarity). The growth of the perturbation is also limited due to lack of multiplication of number of radicals, because each reaction ejects only one radical.

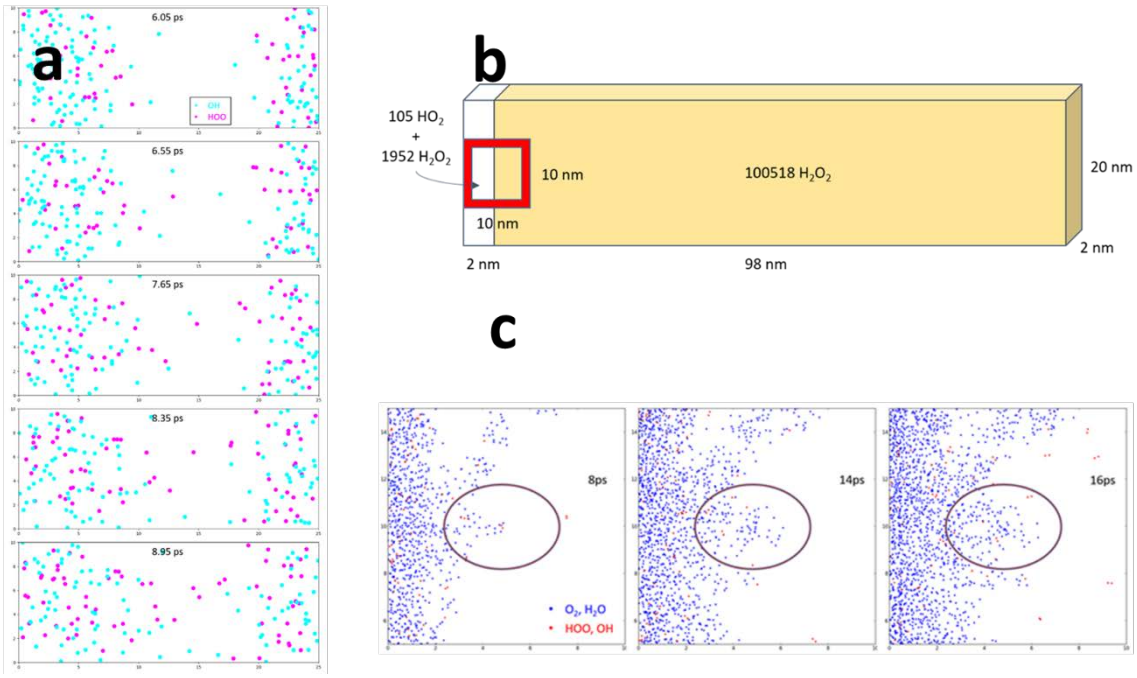


**Figure S4.** (a) Evolution of Case 4; (b) Geometry of Case 4 and (c) Formation and dissipation of perturbation at the interface in Case 9.

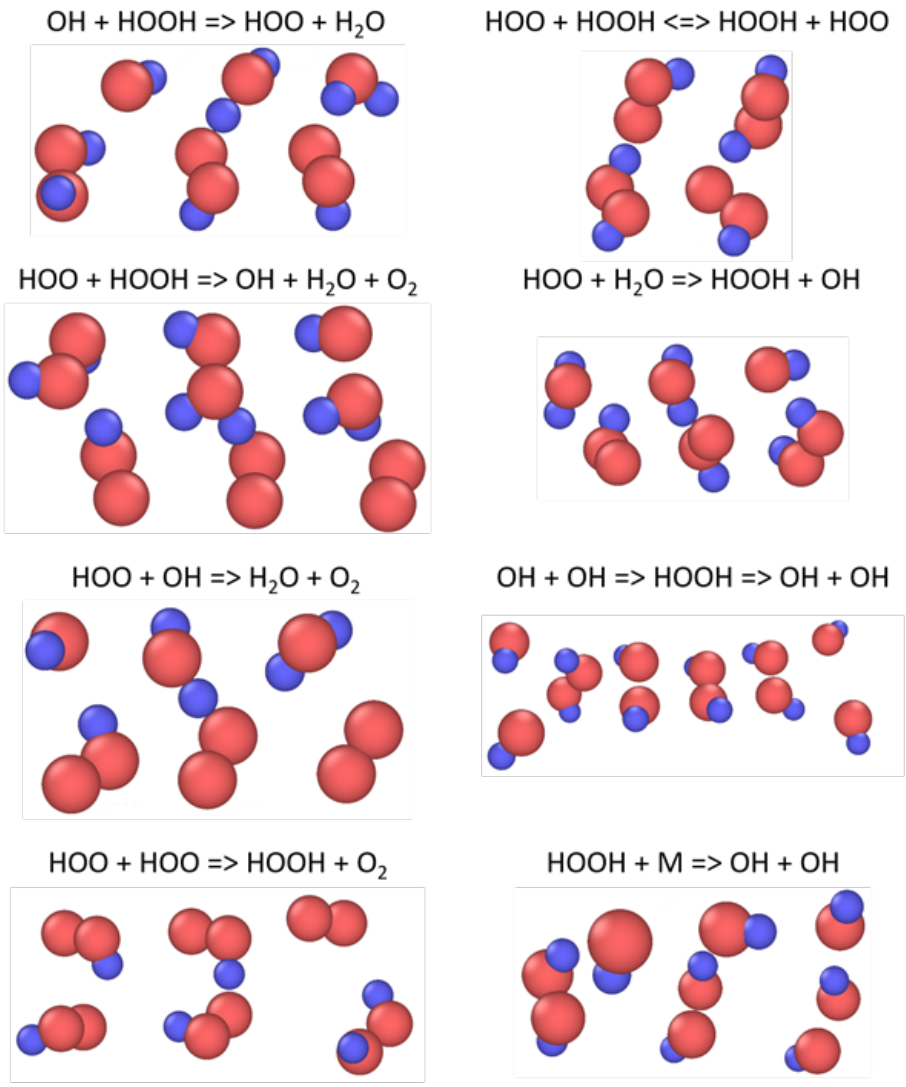


**Figure S5.** Dominant reactions.

Figure S5 shows snapshots of the reactants, transitions states, and products of all dominant reactions present in the HOOH system seeded with OH (Table 1 of the manuscript). These are also available as videos (Videos S1-S7).

**The Haber-Weiss-Willstatter reaction.**

Reaction 2

$$HOO\bullet + H_2O_2 \rightarrow O_2 + H_2O + HO\bullet$$

is well known in the literature. The entire reaction starting from the 2A" state of HOO• and ending with the $^3\Sigma_g$ state of $O_2$ and the $^2\Pi$ state HO• is exothermic by 19.5 kcal/mol. This reaction was discovered in the 1930's by Haber, Weiss and Willstatter in their studies of the decomposition of hydrogen peroxide by iron cations, specifically it was a propagation step[1,2]. This reaction has been referenced often since then with many references[3]. But there has been some debate as to whether the similar reaction

$$OO^- + H_2O_2 \rightarrow O_2 + HO^- + HO\bullet \quad (6)$$

produces the $^1\Delta_g$ or $^3\sum_g^-$ state of dioxygen.

**Quantum Mechanics Calculations of Reaction 2**

We combined the reactants into one system and optimized the geometry was again as a doublet spin state (S=1/2). The binding energy of the reactant complex is -8.4 kcal/mol. Likewise the binding energy of the products with a. doublet spin multiplicity (relative to the initial state) is -25.3 kcal/mol. Using the optimized geometries for the reactant and product, we calculated a doublet transition state along the pathway (Figure S6) that has one negative Hessian eigenvalue. The structure of the transition state is in Figure S7 and he energies are shown in Figure S8. The details of its geometry are in Figure S9.

The energy of this transition state is uphill 14.0 kcal/mol (relative to the initial state). As the reaction proceeds toward the TS, the O2-H1 bond length increases while the H1-O3 bond length decreases (corresponding the hydrogen atom transfer) and simultaneously the O3-O4 bond length increases. The spin state of the system remains a doublet, but the spin pairing changes to become the spin=1 (triplet) state of the dioxygen product while the unpaired spin on the hydroxyl product is coupled to form an overall doublet product (spin-allowed).

**Details of QM calculations.**

All geometries and energies were computed using the B3LYP(7–11) functional with the 6-311G**++(12–15) basis set implemented in the Schrodinger Jaguar software(16).

Separately, the reactant and product structures of HOO•, $H_2O_2$, $O_2$, $H_2O$, and HO• were optimized in order to minimize the energy of the system. In combinations, these express the energy of the reactants and the products held infinitely apart.

**ReaxFF Calculations of Reaction 2**

Using the ReaxFF reactive force field, we obtained an energy barrier of 16.42 kcal/mol for the TS geometry in Figure. S7.

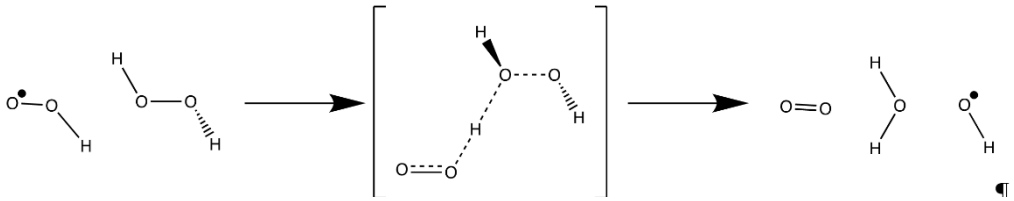

**Figure S6.** Mechanism for Reaction 2, the propagation step in the decomposition of hydrogen peroxide, based on QM calculations.

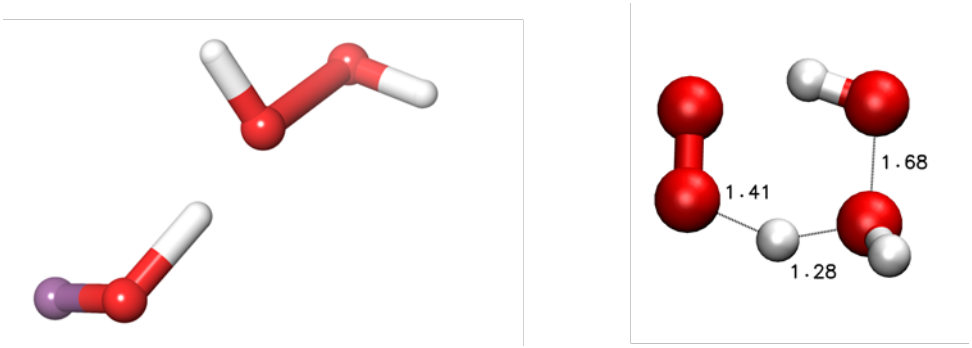


**Figure S7.** The geometry at the TS for Reaction 2 from (left) QM calculations (right) ReaxFF calculations

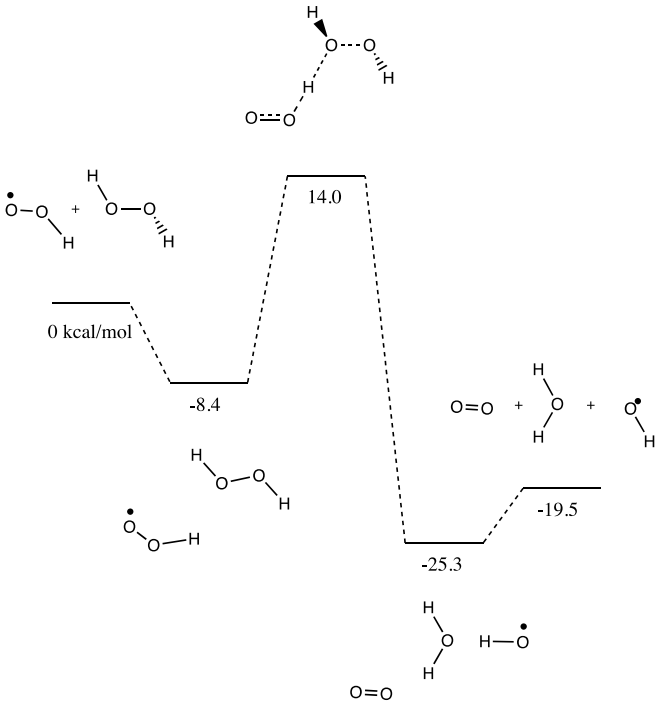


**Figure S8.** The energy surface for Reaction 2 from QM (DFT B3LYP), see Methods.

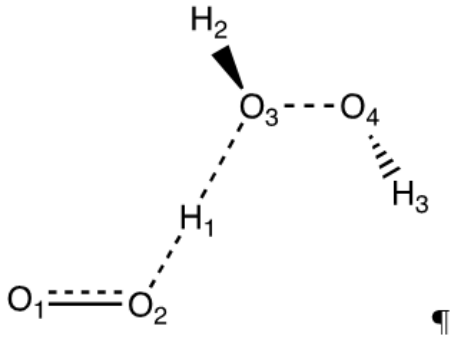


| Bond¤ | Distance·(Å)¤ |
|---|---|
| $O_1$-$O_2$¤ | 1.2712¤ |
| $O_2$-$H_1$¤ | 1.1953¤ |
| $H_1$-$O_3$¤ | 1.1949¤ |
| $H_2$-$O_3$¤ | 0.9685¤ |
| $O_3$-$O_4$¤ | 1.7233¤ |
| $O_4$-$H_3$¤ | 0.9702¤ |

**Figure S9.** Details of the QM transition State for Reaction 2

**Table S1. Bond order cutoffs.**

| Bond | Bond Order Cutoff |
|---|---|
| O-O | 0.300 |
| H-H | 0.300 |
| O-H | 0.300 |

**Movie S1.** 3D animation of HOOH + OH reaction using position data from ReaxFF RMD.

**Movie S2.** 3D animation of HOOH + HOO reaction using position data from ReaxFF RMD.

**Movie S3.** 3D animation of HOO—H—OOH interaction using position data from ReaxFF RMD.

**Movie S4.** 3D animation of HOO + OH reaction using position data from ReaxFF RMD.

**Movie S5.** 3D animation of HOO + HOO reaction using position data from ReaxFF RMD.

**Movie S6.** 3D animation of HOO + $H_2O$ reaction using position data from ReaxFF RMD.

**Movie S7.** 3D animation of HOOH decomposition into OH + OH using position data from ReaxFF RMD.

**Movie S8.** 3D animation of OH + OH interaction using position data from ReaxFF RMD.

**References for SI**


1 Landau L (1944) On the theory of slow combustion. *Acta Physiochim* 19.

2 Sivashinsky G (1983) Instabilities, pattern formation, and turbulence in flames. *Annu. Rev. Fluid Mech.*15:179-199.

3 Haber, F.; Weiss, J. (1934) The Catalytic Decomposition of Hydrogen Peroxide by Iron Salts. *Proc R Soc Lond A, 147* (861), 332–351.

4 Haber, F.; Willstätter, R. Unpaarigkeit Und Radikalketten Im (1931) Reaktions mechanismus Organischer Und Enzymatischer Vorgänge. *Berichte Dtsch. Chem. Ges. B Ser., 64* (11), 2844–2856.

5 Stefan, M. I.; Hoy, A. R.; Bolton, J. R. (1996) Kinetics and Mechanism of the Degradation and Mineralization of Acetone in Dilute Aqueous Solution Sensitized by the UV Photolysis of Hydrogen Peroxide. *Environ. Sci. Technol., 30* (7), 2382–2390.

6 Khan, A. U.; Kasha, M. Singlet (1994) Molecular Oxygen in the Haber-Weiss Reaction. *Proc. Natl. Acad. Sci., 91* (26), 12365–12367.

7 Slater, J. C.; Phillips, J. C. (1974) Quantum Theory of Molecules and Solids Vol. 4: The Self-Consistent Field for Molecules and Solids. *Phys. Today, 27*, 49.

8 Vosko, S. H.; Wilk, L.; Nusair, M. (1980) Accurate Spin-Dependent Electron Liquid Correlation Energies for Local Spin Density Calculations: A Critical Analysis. *Can. J. Phys., 58* (8), 1200–1211.

9 Becke, A. AD Becke, Phys. Rev. A 38, 3098 (1988). *Phys Rev A, 38*, 3098.

10 Lee, C.; Yang, W.; Parr, R. G. (1988) Development of the Colle-Salvetti Correlation-Energy Formula into a Functional of the Electron Density. *Phys. Rev. B, 37* (2), 785.

11 Miehlich, B.; Savin, A.; Stoll, H.; Preuss, H. (1989) Results Obtained with the Correlation Energy Density Functionals of Becke and Lee, Yang and Parr. *Chem. Phys. Lett., 157* (3), 200–206.

12 Clark, T.; Chandrasekhar, J.; Spitznagel, G. W.; Schleyer, P. V. R. (1983) Efficient Diffuse Function-Augmented Basis Sets for Anion Calculations. III. The 3-21+G Basis Set for First-Row Elements, Li–F. *J. Comput. Chem. 4* (3), 294–301.

13 Frisch, M. J.; Pople, J. A.; Binkley, J. S. (1984) Self-Consistent Molecular Orbital Methods 25. Supplementary Functions for Gaussian Basis Sets. *J. Chem. Phys., 80* (7), 3265–3269.

14 Krishnan, R.; Binkley, J. S.; Seeger, R.; Pople, J. A. (1980) Self-consistent Molecular Orbital Methods. XX. A Basis Set for Correlated Wave Functions. *J. Chem. Phys., 72* (1), 650–654.

15 McLean, A. D.; Chandler, G. S. (1980) Contracted Gaussian Basis Sets for Molecular Calculations. I. Second Row Atoms, Z=11–18. *J. Chem. Phys., 72* (10), 5639–5648.

16 Bochevarov, A. D.; Harder, E.; Hughes, T. F.; Greenwood, J. R.; Braden, D. A.; Philipp, D. M.; Rinaldo, D.; Halls, M. D.; Zhang, J.; Friesner, R. A. (2013) Jaguar: A High-Performance Quantum Chemistry Software Program with Strengths in Life and Materials Sciences. *Int. J. Quantum Chem.*, *113* (18), 2110–2142.